

Collective Excitations and Pairing Effects in Drip-Line Nuclei

— *Continuum RPA in Coordinate-Space HFB* —

Masayuki MATSUO ^{*)}

*Graduate School of Science and Technology, Niigata University, Niigata, 950-2181,
Japan*

(Received)

We discuss novel features of a new continuum RPA formulated in the coordinate-space Hartree-Fock-Bogoliubov framework. This continuum quasiparticle RPA takes into account both the one- and two-particle escaping channels. The theory is tested with numerical calculations for monopole, dipole and quadrupole excitations in neutron-rich oxygen isotopes near the drip-line. Effects of the particle-particle RPA correlation caused by the pairing interaction are discussed in detail, and importance of the selfconsistent treatment is emphasized.

§1. Introduction

Collective excitation in unstable nuclei is one of the most attractive subjects since the exotic structures in the ground state, such as halo, skin, and the presence of loosely bound nucleons, may cause new features in the excitations, e.g. the low-energy dipole mode that is being discussed extensively. The random phase approximation (RPA) or the linear response theory is one of the most powerful framework to investigate such problems microscopically. Indeed the continuum RPA theory in the coordinate-space representation^{1),2)} has played major roles so far since it can describe the continuum states crucial for nuclei near drip-line.³⁾⁻⁵⁾

The pairing correlation is another key feature of drip-line nuclei.⁶⁾⁻⁸⁾ To treat the coupling of the continuum states as well as the density dependence of the pairing correlation, the Hartree-Fock-Bogoliubov (HFB) theory formulated in the coordinate-space representation^{6),9)} has been developed while the conventional BCS approximation has inherent deficiency.

It is therefore important to combine the continuum RPA and the coordinate space HFB in a consistent way in order to describe the excitations in unstable nuclei near drip-line, especially when the pairing correlation play crucial roles. We have recently shown that a new quasiparticle RPA (QRPA) satisfying this requirement is indeed possible.¹⁰⁾ In the present paper, we discuss characteristic features of the theory and analyze excitations of near-drip-line nuclei, focusing on effects of the pairing, by using numerical calculations performed for the monopole, dipole and quadrupole excitations in neutron-rich oxygen isotopes. The previous continuum QRPA approaches employ the BCS approximation.¹¹⁾⁻¹⁴⁾ Other QRPA approaches applied to unstable nuclei neglect the escaping effects since some use the BCS quasiparticle basis,¹⁵⁾⁻¹⁷⁾ and other adopt the coordinate-space HFB but use the discretized canonical basis.¹⁸⁾ The present formalism provides the first consistent continuum

^{*)} E-mail address: matsuo@nt.sc.niigata-u.ac.jp

QRPA approach for the drip-line nuclei with pairing correlation.

§2. Continuum RPA in coordinate-space HFB

The Hartree-Fock-Bogoliubov theory describes the pairing correlation in terms of quasiparticles and selfconsistent mean-fields including the pairing potential. To correctly describe behavior of the quasiparticles in the surface and exterior regions related to halo or skin, it is preferable to solve the HFB equation in the coordinate-space representation^{6), 9)}

$$\mathcal{H}_0\phi_i(\mathbf{r}\sigma) = E_i\phi_i(\mathbf{r}\sigma), \quad (2.1)$$

which determines the quasiparticle states and the associated two-component wave functions

$$\phi_i(\mathbf{r}\sigma) \equiv \begin{pmatrix} \varphi_{1,i}(\mathbf{r}\sigma) \\ \varphi_{2,i}(\mathbf{r}\sigma) \end{pmatrix}. \quad (2.2)$$

Here the HFB mean-field Hamiltonian is expressed in a 2×2 matrix form

$$\mathcal{H}_0(\mathbf{r}\sigma, \mathbf{r}'\sigma') \equiv \begin{pmatrix} h(\mathbf{r}\sigma, \mathbf{r}'\sigma') - \lambda\delta(\mathbf{r} - \mathbf{r}')\delta_{\sigma\sigma'} & \tilde{h}(\mathbf{r}\sigma, \mathbf{r}'\sigma') \\ \tilde{h}^*(\mathbf{r}\tilde{\sigma}, \mathbf{r}'\tilde{\sigma}') & -h^*(\mathbf{r}\tilde{\sigma}, \mathbf{r}'\tilde{\sigma}') + \lambda\delta(\mathbf{r} - \mathbf{r}')\delta_{\sigma\sigma'} \end{pmatrix} \quad (2.3)$$

where h includes the kinetic energy and the Hartree-Fock field in the particle-hole (ph) channel and \tilde{h} is the selfconsistent pairing field in the particle-particle (pp) channel. They are expressed in terms of the effective two-body interactions and the normal and pair densities although we omit here their detailed expression. Properties of the static HFB equations and techniques to solve them are known.^{6), 9)} The quasiparticle excitation energy E_i is defined with respect to the Fermi energy $\lambda (< 0)$. The spectrum becomes continuous for $E_i > |\lambda|$ and the quasiparticles above the threshold energy $|\lambda|$ can escape from the nucleus. This is a special feature we have to take care of when we describe weakly bound systems with pairing correlation.

In order to describe the linear response of the system, we need to know the motion of two quasiparticles propagating under the HFB mean-field Hamiltonian. Assuming that the external field and the selfconsistent field are the local one-body fields expressed in terms of the normal density $\rho(\mathbf{r}) = \sum_{\sigma} \psi^{\dagger}(\mathbf{r}\sigma)\psi(\mathbf{r}\sigma)$ and the pair densities $\tilde{\rho}_{\pm}(\mathbf{r}) = \frac{1}{2} \sum_{\sigma} \left(\psi(\mathbf{r}\tilde{\sigma})\psi(\mathbf{r}\sigma) \pm \psi^{\dagger}(\mathbf{r}\sigma)\psi^{\dagger}(\mathbf{r}\tilde{\sigma}) \right)$, it is enough to consider response function for these operators. The unperturbed response function $R_0(\omega)$ at frequency ω , that neglects effect of the residual interaction, is easily derived from a time-dependent extension of Eq.(2.1) as

$$R_0^{\alpha\beta}(\mathbf{r}, \mathbf{r}', \omega) = \frac{1}{2} \sum_i \sum_{\sigma\sigma'} \left\{ \bar{\phi}_i^{\dagger}(\mathbf{r}\sigma) \mathcal{A} \mathcal{G}_0(\mathbf{r}\sigma, \mathbf{r}'\sigma', -E_i + \hbar\omega + i\epsilon) \mathcal{B} \bar{\phi}_i(\mathbf{r}'\sigma') \right. \\ \left. + \bar{\phi}_i^{\dagger}(\mathbf{r}'\sigma') \mathcal{B} \mathcal{G}_0(\mathbf{r}'\sigma', \mathbf{r}\sigma, -E_i - \hbar\omega - i\epsilon) \mathcal{A} \bar{\phi}_i(\mathbf{r}\sigma) \right\} \quad (2.4)$$

with use of the HFB Green function $\mathcal{G}_0(E + i\epsilon) = (E + i\epsilon - \mathcal{H}_0)^{-1}$ and the wave functions $\bar{\phi}_i(\mathbf{r}\sigma)$ of the quasiparticle states. Here $\bar{\phi}_i(\mathbf{r}\sigma)$ is the one associated with the negative energy quasiparticle state (with energy $-E_i$) conjugate to a positive

energy state $\phi_i(\mathbf{r}\sigma)$ with E_i . The index α, β and the symbol \mathcal{A}, \mathcal{B} refer to the three kinds of densities $\rho, \tilde{\rho}_+$ and $\tilde{\rho}_-$. Structure of Eq.(2.4) is similar to the familiar form for unpaired systems¹⁾ except that we here use the quasiparticle wave functions and the HFB Green function. However this expression is not satisfactory since the summation \sum_i assumes that all the quasiparticle states belong to a discrete spectrum. We have to take a continuum limit of this summation to deal with the continuum effects accurately.

The continuum limit is introduced by first replacing the summation with a contour integral of the HFB Green function $\mathcal{G}_0(E)$ in the complex E plane. The contour is chosen so that it encloses all the quasiparticle poles at $-E_i$ of the negative energy quasiparticle states (see, Fig.1). By doing this, the unperturbed response function can be expressed as

$$R_0^{\alpha\beta}(\mathbf{r}, \mathbf{r}', \omega) = \frac{1}{4\pi i} \int_C dE \sum_{\sigma\sigma'} \{ \text{Tr} \mathcal{A} \mathcal{G}_0(\mathbf{r}\sigma, \mathbf{r}'\sigma', E + \hbar\omega + i\epsilon) \mathcal{B} \mathcal{G}_0(\mathbf{r}'\sigma', \mathbf{r}\sigma, E) \\ + \text{Tr} \mathcal{A} \mathcal{G}_0(\mathbf{r}\sigma, \mathbf{r}'\sigma', E) \mathcal{B} \mathcal{G}_0(\mathbf{r}'\sigma', \mathbf{r}\sigma, E - \hbar\omega - i\epsilon) \} \quad (2.5)$$

in terms of products of the HFB Green function \mathcal{G}_0 and their integral. Now we can implement the continuum quasiparticle spectrum by adopting the exact HFB Green function which satisfies the proper boundary condition of outgoing wave for the continuum states.⁹⁾ The exact HFB Green function has poles on the real E axis in the interval $-|\lambda| < E < |\lambda|$, corresponding to the discrete bound quasiparticle states, and has the branch cuts, associated with the continuum states, along the real axis for $E > |\lambda|$ and $E < -|\lambda|$ (Fig.1). We incorporate in this way the continuum states within the framework.

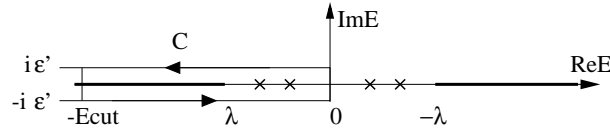


Fig. 1. The contour C in the integral representation of the response function. The crosses represent the poles at $E = \pm E_i$ corresponding to the discrete bound quasiparticle states. The thick lines are the branch cuts associated with the continuum states. The imaginary part ϵ' must satisfy the condition $0 < \epsilon' < \epsilon$.

Having the continuum unperturbed response function $R_0(\omega)$, we are then able to take into account the RPA correlation caused by the residual interactions. The RPA linear response equation for the transition densities at frequency ω reads

$$\begin{pmatrix} \delta\rho(\mathbf{r}, \omega) \\ \delta\tilde{\rho}_+(\mathbf{r}, \omega) \\ \delta\tilde{\rho}_-(\mathbf{r}, \omega) \end{pmatrix} = \int d\mathbf{r}' \begin{pmatrix} R_0^{\alpha\beta}(\mathbf{r}, \mathbf{r}', \omega) \end{pmatrix} \begin{pmatrix} \kappa_{ph}(\mathbf{r}')\delta\rho(\mathbf{r}', \omega) + v^{ext}(\mathbf{r}') \\ \kappa_{pp}(\mathbf{r}')\delta\tilde{\rho}_+(\mathbf{r}', \omega) \\ -\kappa_{pp}(\mathbf{r}')\delta\tilde{\rho}_-(\mathbf{r}', \omega) \end{pmatrix} \quad (2.6)$$

where $\kappa_{ph}(\mathbf{r})$ and $\kappa_{pp}(\mathbf{r})$ are the residual interactions in the ph- and pp-channels. The strength function for the external one-body field $v^{ext}(\mathbf{r})$ is evaluated as $f(\omega) = -\frac{1}{\pi} \text{Im} \int d\mathbf{r} v^{ext}(\mathbf{r})^* \delta\rho(\mathbf{r}, \omega)$.

An important feature of the present continuum QRPA is that the linear response equation (2.6) takes into account the pair transition density $\delta\tilde{\rho}_{\pm}$ as well as the normal transition density $\delta\rho$. Note that the three transition densities couple since the system has pairing correlation. By solving Eq.(2.6), the RPA correlations responsible for the excited states, represented by the ring diagram, are taken into account both in the ph-channel (through $\delta\rho$) and in the pp-channel ($\delta\tilde{\rho}_{\pm}$). The particle-particle RPA correlation may be called the *dynamical pairing correlation* to distinguish from the pairing correlation already taken into account as the quasiparticles in the HFB description of the ground state. We demonstrate in the following important roles played by the dynamical pairing correlation for excitations of nuclei near drip-line.

Another novel aspect of the theory concerns with the continuum states. The two-quasiparticle states appearing in the QRPA formalism are classified in three groups; the first consists of two nucleons both occupying the bound discrete quasiparticle states, the second with one particle in the bound states and the other in the continuum states, and the last with two particles both in the continuum states. The three configurations are incorporated through the product of two HFB Green function \mathcal{G}_0 appearing in Eq.(2.6) since \mathcal{G}_0 describes exactly both the discrete and continuum states. Thus the present linear response theory contains both the channel of one-nucleon escaping and that of two-nucleon emission. The threshold energy for the two-nucleon channel is twice the Fermi energy $E_{th,2} = 2|\lambda|$, while the threshold for one-nucleon escape is $E_{th,1} = |\lambda| + E_{i,min}$ where $E_{i,min}$ is the lowest of the quasiparticle energy E_i . See Ref.10) for details of the formalism.

§3. Numerical analysis for oxygen isotopes

3.1. Monopole: pairing selfconsistency

In the following, we present our numerical analysis performed for the neutron-rich even-even oxygen isotopes including the neutron drip-line nucleus ^{24}O . The adopted model assumes the Woods-Saxon potential for the single-particle potential. As for the residual interaction in the ph-channel, the Skyrme-type density-dependent delta force $v_{ph}(\mathbf{r}, \mathbf{r}') = (t_0(1 + x_0P_{\sigma}) + t_3(1 + x_3P_{\sigma})\rho(r))\delta(\mathbf{r} - \mathbf{r}')$ is used. The model parameters for the Woods-Saxon potential and the Skyrme force are taken the same as Shlomo-Bertsch.¹⁾ (Note that the adopted Woods-Saxon parameters are slightly different from those in Ref.10.) Although this modeling of the potential and the ph-interaction is not selfconsistent, an approximate selfconsistency is satisfied by renormalizing the interaction strength t_0 and t_1 with an overall factor f so that the dipole response has a zero-energy mode corresponding to the spurious center of mass motion.¹⁾

For the pairing interaction, we adopt the density-dependent delta force^{8),19)}

$$v_{pair}(\mathbf{r}, \mathbf{r}') = \frac{1}{2}V_0(1 - P_{\sigma})(1 - \rho(r)/\rho_0)\delta(\mathbf{r} - \mathbf{r}'), \quad (3.1)$$

with $\rho_0 = 0.16 \text{ fm}^{-3}$. We use the same force to obtain the HFB pairing field for the ground state and also to solve the linear response equation for the excitations. Thus the calculation is selfconsistent in the pp-channel.

The pairing force strength V_0 is fixed to a value $V_0 = 520 \text{ fm}^{-3} \text{ MeV}$ which gives an average neutron pairing gap $\langle \Delta \rangle$ (see Ref.10) for its definition) reproducing the global trend $\langle \Delta \rangle \approx 12/\sqrt{A} \text{ MeV}$ in $^{18,20}\text{O}$. The calculated value is $\langle \Delta \rangle = 2.37, 2.83, 2.84, 2.89 \text{ MeV}$ for neutron and zero gap for proton in $^{18-24}\text{O}$. The model parameters and the procedure of calculation is the same as those in Ref.10) except the small difference in the Woods-Saxon parameters and the force renormalization factor, which is $f = 0.689, 0.704, 0.750, 0.775$ for $^{18-24}\text{O}$. Using the present parameters, the peak energies of the giant quadrupole and dipole resonances are lifted by about a few MeV (cf. Fig.3 compared with Fig.2 in Ref.10)), giving better description of GR's in ^{16}O . The calculation will be further improved if we use the Hartree-Fock potential for the ph-part. We will not discuss here quantitative (dis)agreement with the experiments,^{16), 23) - 26)} but rather focus on qualitative aspects seen in the theoretical analysis. The small imaginary part in the response function is fixed to $\epsilon = 0.2 \text{ MeV}$. It has an effect to bring an additional width of 0.4 MeV in the calculated strength function.

Let us first emphasize importance of the selfconsistent treatment of the pairing in the linear response equation by looking into the Nambu-Goldstone mode associated with the nucleon number conservation. Fig.2 shows the monopole strength function for the neutron number operator $\hat{N} = \int d\mathbf{r} \sum_{\sigma} \psi^{\dagger}(\mathbf{r}\sigma)\psi(\mathbf{r}\sigma)$. There should be no response to the number operator since it is the conserved quantity. The calculated strength function (solid line) exhibits this feature, and there is essentially no spurious excitation that could have been caused by the nucleon number mixing in the HFB ground state. Note that the spurious strength for \hat{N} were induced if we took into account the pairing correlation only in the static mean-field and neglected the dynamical pairing correlation i.e. neglecting the pairing interaction in the linear response equation (2.6) (see the dotted curve in Fig.2). In the selfconsistent calculation the Nambu-Goldstone mode has an excitation energy very close to zero. We can shift this excitation energy to exact zero by modifying the pairing force strength V_0 in Eq.(2.6) just by less than 1%, indicating that a good accuracy for the pairing selfconsistency is obtained in the actual calculation.

3.2. Quadrupole excitation

The strength functions for the proton, neutron, isoscalar, and isovector quadrupole operators calculated for the drip-line nucleus ^{24}O are shown in Fig.3. The peak around $E \approx 18 \text{ MeV}$ in the isoscalar strength and the broad distribution

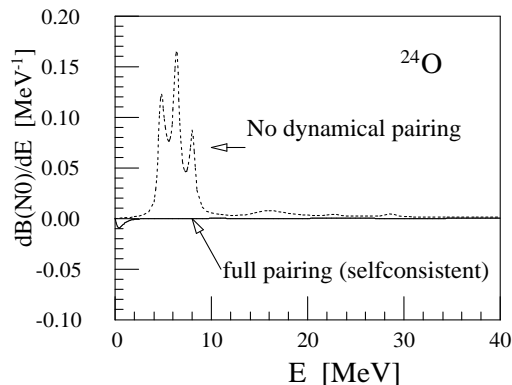


Fig. 2. The strength function for the neutron number operator in ^{24}O .

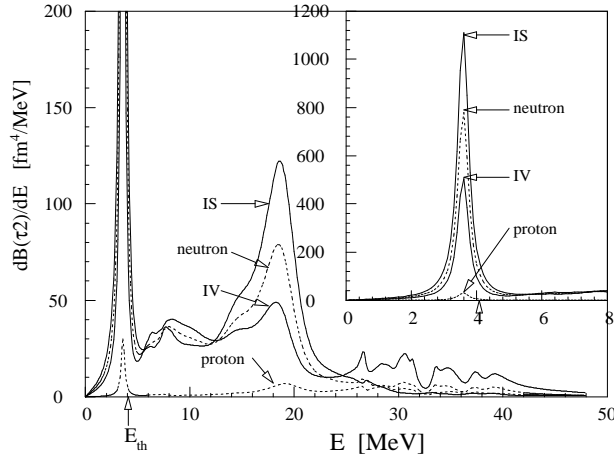


Fig. 3. The strength functions for the isoscalar, isovector, proton and neutron quadrupole moments in ^{24}O . The threshold energy $E_{th,1n} = E_{th,2n} = 2|\lambda| = 4.08$ MeV for neutron emission is indicated by an arrow.

around $E \approx 25 - 40$ MeV of the isovector strength correspond to the isoscalar and isovector giant quadrupole resonances, respectively, although isoscalar and isovector characters are mutually mixed. The most prominent feature is presence of the intense low-lying state at $E = 3.6$ MeV, which is very close to the threshold energy $E_{th,1n} = E_{th,2n} = 4.08$ MeV for the one- and two-neutron escape. This low-lying 2^+ state has large neutron strength which is overwhelming the proton strength. The energy weighted sum of the neutron (and the isoscalar) strength in this state amounts to 12 (13)% of the sum-rule value. The neutron transition density $\delta\rho(r)$ has a large peak in the surface region. Thus this low-lying state has a characteristic of neutron surface vibration; for which the dominance of neutron strength marks significant difference from the isoscalar low-lying 2^+ states in the stable nuclei. (The slightly lower excitation energy and the weaker strength of the low-lying 2^+ state in comparison with the calculation in

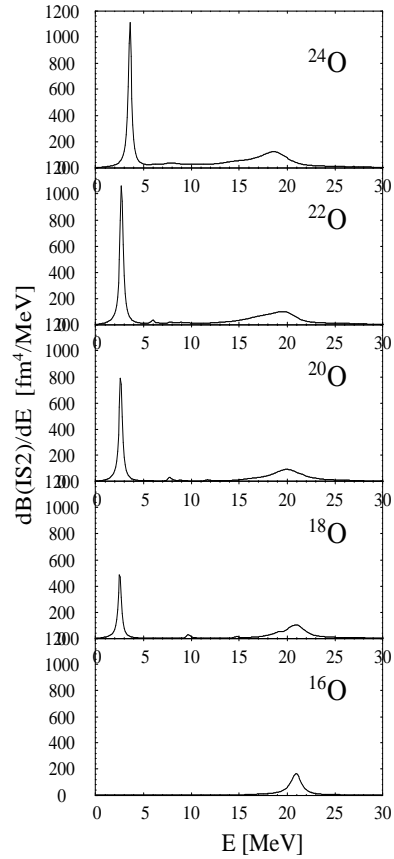


Fig. 4. Isoscalar quadrupole strength function for $^{16-24}\text{O}$.

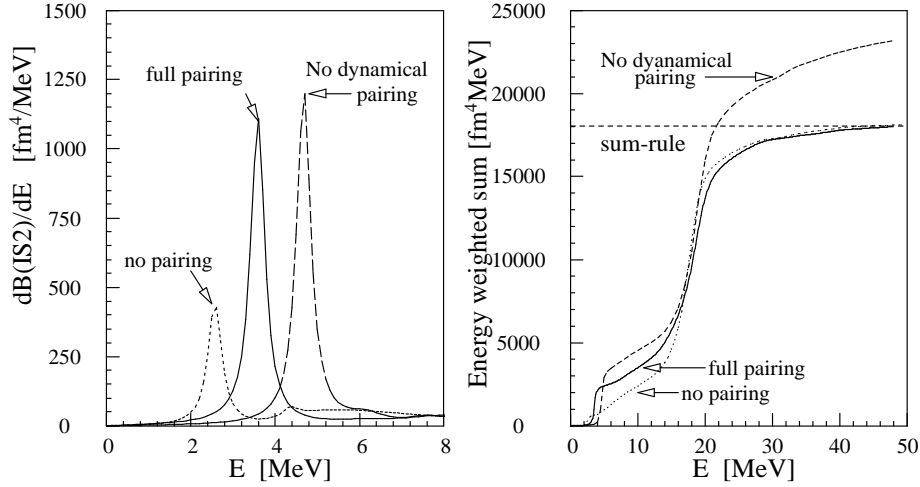


Fig. 5. Isoscalar quadrupole strength function in ^{24}O (left) and its energy weighted sum (right). The calculation with the full pairing effects (solid) is compared with the one with no pairing effects (dotted), and the one where only the static HFB potential is taken into account and the dynamical pairing effect is neglected (dashed).

Ref.10) are due to the different Woods-Saxon parameter.)

Figure 4 shows systematics of the isoscalar quadrupole strength for $^{16-24}\text{O}$. The isoscalar strength (and the neutron strength not shown here) of the low-lying 2^+ state increases with the neutron number. The $B(E2)$ value of this state, on the other hand, is not very dependent of the neutron number; $B(E2) = 17, 18, 20, 18 e^2\text{fm}^4$ for $A = 18 - 24$. Thus the neutron character of this vibration mode is enhanced as the drip-line is approached. Significant amount of neutron strength in the interval between the low-lying 2^+ state and the GQR, seen in the near-drip-line nuclei $^{22,24}\text{O}$, arises from the neutron continuum states. It is also seen that the width of the isoscalar giant quadrupole resonance increases with the neutron number. This can be naturally interpreted as an increase of the neutron escaping width.

Effects of neutron pairing on the quadrupole response are quite large. The pairing correlation increases drastically the collectivity of the low-lying 2^+ state, as shown in Fig.5 (solid vs. dotted curves). The energy weighted isoscalar sum $S(\text{IS2}) = \int E \left(\frac{dB(\text{IS2})}{dE} \right) dE$ of the 2^+ state (and the E2 sum $S(E2)$) is calculated to be 730, 1220, 1680, 2330 fm^4MeV (and 43, 47, 54, 62 $e^2\text{fm}^4\text{MeV}$) for $A = 18-24$, while by neglecting the pairing correlations these quantities become 73, 132, 277, 646 fm^4MeV (and 3, 4, 7, 14 $e^2\text{fm}^4\text{MeV}$), which are several times smaller. Here we emphasize that the total pairing effect arises not only from the static HFB mean-field but also from the dynamical RPA correlation induced by the pairing interaction. As Fig.5 (left) indicates, the dynamical pairing correlation lowers the excitation energy of the 2^+ state by ≈ 1 MeV (solid vs. dashed curves).

The dynamical pairing correlation has another important role as shown in Fig.5 (right), where accumulated energy weighted isoscalar sum $\int_0^E E' \left(\frac{dB(\text{IS2})}{dE'} \right) dE'$ is plotted. Note that the energy weighted sum rule is satisfied quite accurately, but this

is achieved only by including selfconsistently the dynamical pairing correlation on top of the mean-field pairing effect. If one neglects the dynamical pairing, the selfconsistency in the linear response equation is broken and the sum rule is violated as seen for the dashed curve.

3.3. Dipole excitation

The dipole excitation is very interesting since the microscopic structure of the low-energy E1 mode, called often the soft dipole mode or the pygmy dipole resonance, is currently debated (3), 7), 20) - 22), 26) while a large effect of the pairing correlation on this mode is also pointed in the case of the halo nucleus ^{11}Li .⁸⁾ We here calculate the electric dipole strength by using the operator $D_\mu = e\frac{Z}{A}\sum_n rY_{1\mu}(n) - e\frac{N}{A}\sum_p rY_{1\mu}(p)$, from which the center of mass motion is explicitly removed. The result is shown in Fig.6. As the neutron number increases the E1 strength in the low energy region (e.g. $E < 15$ MeV) develops significantly; the energy weighted sum below 15 MeV is $S(E1) = 7, 11, 16, 21\%$ of the TRK sum-rule value for $A = 18-24$. The transition density $\delta\rho(r)$ (shown in Fig.7) indicates that only neutrons are moving in the exterior region, whereas in the surface region neutrons and protons move coherently in the direction opposite to the outside neutrons. Thus the low-energy structure has at least partly the character of the pygmy resonance or the soft dipole mode.^{20), 7)} The low-energy strength may also be related to the so called threshold strength since the strength increases sharply just above the one-neutron threshold $E_{th,1n}$ (see Fig.6). In fact, it cannot be described well by discretizing the neutron continuum states with use of, e.g. a spherical box boundary condition with

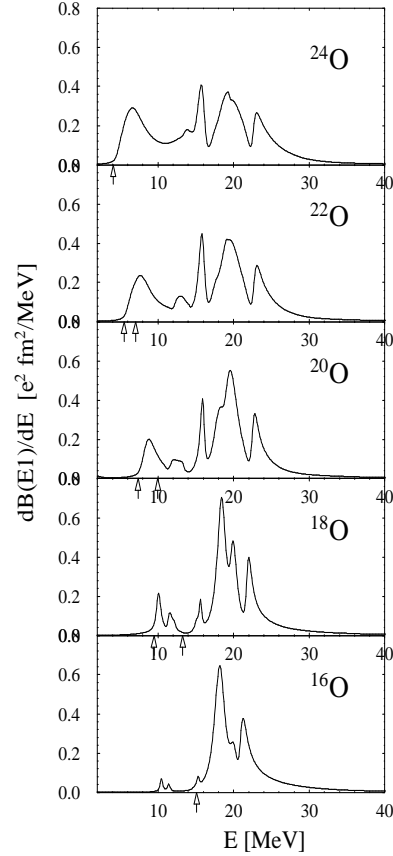


Fig. 6. Electric dipole strength function for $^{16-24}\text{O}$. The arrows indicate the one- and two-neutron thresholds.

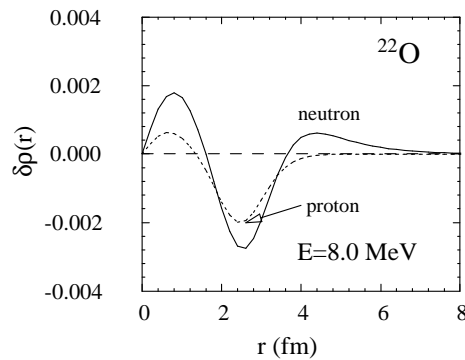


Fig. 7. The transition density for the E1 response of neutron (solid) and proton (dashed) at $E = 8.0$ MeV in ^{22}O , plotted as a function of the radial coordinate r .

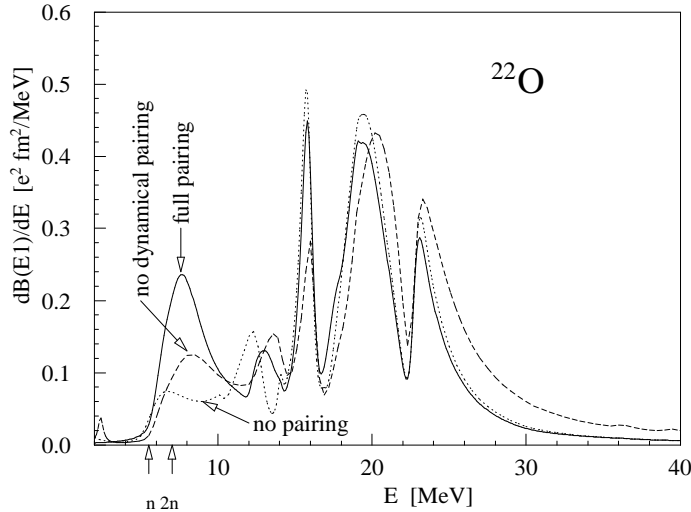


Fig. 8. Effects of the pairing correlations on the dipole response in ^{22}O . The solid curve is obtained with full pairing effects included. For the dotted curve no pairing effect is included whereas in the calculation shown by the dashed curve only the static HFB potential is taken into account and the dynamical pairing effect is neglected. The TRK sum rule is satisfied for the solid and dotted curves, but not for the dashed curve.

a box radius $R = 20$ fm since this is a structure consisting of genuine continuum states. Note however that the low energy strength does not arise purely from unperturbed neutron continuum states, as we see below.

Neutron pairing effect on the E1 strength is strong as shown in Fig.8, where different contributions of the effects are also examined. The total pairing effect enhances the low-energy E1 strength near the threshold $E \sim 8\text{MeV}$. It is also seen that the static mean-field pairing increases the low-energy strength with respect to the unpaired response (dashed vs. dotted curves). This effect may be attributed to partial filling, due to the pairing, of the neutron $2s_{1/2}$ orbit which is influential on the threshold strength. However, more significant is the enhancement caused by the dynamical pairing correlation (solid vs. dashed curves). This indicates that the enhanced low-energy strength is not simply the threshold strength associated with the unperturbed quasi-neutron states occupying the continuum and the weakly bound orbits, but rather it is due to the pairing RPA correlation that mixes different two-quasineutron states. A similar effect is seen in Ref.8) in their analysis of ^{11}Li using a two-neutron continuum shell model.

§4. Conclusions

The new linear response theory formulated in the coordinate-space HFB enables us to describe the collective excitations in nuclei near drip-line where the pairing correlation and the coupling to continuum states are important. The dynamical RPA correlations in the excited states are taken into account both in the ph- and pp-channels in a way consistent with the description of the static HFB mean-field.

The continuum states in the one- and two-particle escaping channels are included. Since the theory satisfies the pairing selfconsistency both in the HFB ground state and in the linear response equation, there is no spurious excitation of nucleon number and the energy weighted sum rule is guaranteed with good accuracy. The dynamical pairing correlation in the pp-channel causes strong enhancement in the strength of the low-lying quadrupole neutron vibration and of the low-energy dipole excitation as demonstrated with the numerical analysis for oxygen isotopes near the neutron drip-line.

References

- 1) S. Shlomo, G. Bertsch, Nucl. Phys. **A243** (1975), 507.
- 2) G.F. Bertsch, S.F. Tsai, Phys. Rep. **18** (1975), 125.
- 3) I. Hamamoto, H. Sagawa, X.Z. Zhang, Phys. Rev. **C57** (1998), R1064; Nucl. Phys. **A648** (1999), 203.
I. Hamamoto, in this proceedings.
- 4) S.A. Fayans, Phys. Lett. **B267** (1991), 443.
- 5) F. Ghielmetti, G.Colò, E. Vigezzi, P.F. Bortignon, R.A. Broglia, Phys. Rev. **C54** (1996), R2143.
- 6) J. Dobaczewski, H. Flocard, J. Treiner, Nucl. Phys. **A422** (1984), 103.
J. Dobaczewski, W. Nazarewicz, T.R. Werner, J.F. Berger, C.R. Chinn, J. Dechargé, Phys. Rev. **C53** (1996), 2809.
S. Mizutori, J. Dobaczewski, G.A. Lalazissis, W. Nazarewicz, P.-G. Reinhard, Phys. Rev. **C61** (2000), 044326.
J. Dobaczewski, in this proceedings.
- 7) P.G. Hansen, B. Jonson, Europhys. Lett. **4** (1987), 409.
- 8) G.F. Bertsch, H. Esbensen, Ann. Phys. **209** (1991), 327.
H. Esbensen, G.F. Bertsch, Nucl. Phys. **A542** (1992), 310.
- 9) S.T. Belyaev, A.V. Smirnov, S.V. Tolokonnikov, S.A. Fayans, Sov. J. Nucl. Phys. **45** (1987), 783.
- 10) M. Matsuo, Nucl. Phys. **A696** (2001), 371.
- 11) A.P. Platonov, E.E. Saperstein, Nucl. Phys. **A486** (1988), 63.
- 12) I.N. Borzov, S.A. Fayans, E. Krömer, D. Zawischa, Z. Phys. **A355** (1996), 117.
- 13) S. Kamerdzhiev, R.J. Liotta, E. Litvinova, V. Tselyaev, Phys. Rev. **C58** (1998), 172.
- 14) K. Hagino, H. Sagawa, Nucl. Phys. **A695** (2001), 82.
- 15) E. Khan, Nguyen Van Giai, Phys. Lett. **B472** (2000), 253.
- 16) E. Khan, et al., Phys. Lett. **B490** (2000), 45.
- 17) G. Colò, P.F. Bortignon, Nucl. Phys. **A696** (2001), 427.
- 18) J. Engel, M. Bender, J. Dobaczewski, W. Nazarewicz, R. Surman, Phys. Rev. **C60** (1999), 014302.
M. Bender, J. Dobaczewski, J. Engel, W. Nazarewicz, preprint nucl-th/0112056.
- 19) J. Terasaki, P.-H. Heenen, P. Bonche, J. Dobaczewski, H. Flocard, Nucl. Phys. **A593** (1995), 1.
- 20) Y. Suzuki, K. Ikeda, H. Sato, Prog. Theor. Phys. **83** (1987), 180.
- 21) F. Catara, E.G. Lanza, M.A. Nagarajan, A. Vitturi, Nucl. Phys. **A624** (1997), 449.
- 22) D. Vretenar, N. Paar, P. Ring, G.A. Lalazissis, Nucl. Phys. **A692** (2001), 496.
P. Ring, in this proceedings.
- 23) J.K. Jewell, et al., Phys. Lett. **B454** (1999), 181.
- 24) P.G. Thirolf, et al., Phys. Lett. **B485** (2000), 16.
- 25) F. Azaiez, Phys. Scr. **T88** (2000), 118.
M. Belleguic, et al., Nucl. Phys. **A682** (2001), 136c.
- 26) A. Leistenschneider, et al., Phys. Rev. Lett. **86** (2001), 5442.